Mathematics

https://www.aimspress.com/journal/Math

AIMS Mathematics, 11(7): 22233–22257.
DOI: 10.3934/math.2026900
Received: 26 May 2026
Revised: 06 July 2026
Accepted: 14 July 2026
Published: 24 July 2026

Research article

Variance swap valuation under a Heston jump model with stochastic long-run variance and macro-liquidity feedback

Ke Wang[1], Jing Fu[2,*], Ren-hong Yan[3] and Fan Lei[1]

[1] School of Science, Civil Aviation Flight University of China, No. 46, 4th Section of Nanchang Road, Guanghan City, Sichuan Province, China

[2] School of Mathematics and Statistics, Zhaotong University, Guoxue Road, Zhaoyang District, Zhaotong City, Yunnan Province, China

[3] Research Institute of Economics and Management, Southwestern University of Finance and Economics, No. 555 Liutai Avenue, Wenjiang District, Chengdu City, Sichuan Province, China

* **Correspondence:** E-mail: jingfu307@ztu.edu.cn.

Abstract: This paper develops an affine pricing framework for discretely and continuously monitored variance swaps under a Heston-type stochastic volatility model with finite-activity jumps, stochastic long-run variance, and macro-liquidity feedback. The key modeling feature is that a persistent macro-liquidity state variable enters the mean-reversion target of the spot variance process, so that liquidity conditions affect future expected quadratic variation through the variance target in addition to asset-price or liquidity-discount channels. Under the risk-neutral measure, the four-factor model remains exponentially affine. We derive the joint moment-generating function, the Riccati system, the fair strike for discretely sampled actual-return variance swaps, and the continuous-monitoring limiting strike. We also establish finite-horizon transform admissibility conditions and prove that the discrete actual-return strike converges to the continuous quadratic-variation benchmark as the monitoring mesh vanishes. Numerical experiments show that the proposed model nests the relevant no-liquidity and no-jump benchmarks, that Monte Carlo estimates remain close to the affine-transform prices, and that the macro-liquidity channel raises the benchmark fair strikes by about 1.9% when liquidity stress increases the effective long-run variance target. The results provide a tractable link between stochastic long-run variance modeling, liquidity-adjusted derivative valuation, and jump-sensitive variance swap pricing.

Keywords: variance swaps; stochastic Long-Run variance; Macro-liquidity; moment generating function; closed-form pricing
Mathematics Subject Classification: 91G20

1. Introduction

The valuation of variance swaps is rooted in the theory of realized variation and in the construction of analytically tractable stochastic-volatility models. From the perspective of realized variation, Barndorff-Nielsen [2] shows that realized quadratic variation contains both the integrated diffusive variance and the quadratic contribution of jumps, while bipower variation provides a way to separate the continuous and discontinuous components of price variation. This insight is fundamental for variance swap valuation because the fair strike of a continuously sampled contract depends directly on the expected quadratic variation of the underlying return process. Building on this theoretical foundation, Zhu and Lian [31] derive closed-form pricing formulas for variance swaps under Heston-type stochastic volatility models and show that different definitions of realized variance can be handled within a PDE-based analytical framework. Broadie and Jain [6] further demonstrate that discrete monitoring and price jumps can materially affect fair variance and volatility swap strikes, especially when jump risk is present. More generally, Cui et al. [8] develop a transform-based framework for discretely sampled realized variance derivatives under a broad class of stochastic volatility models with jumps, highlighting the importance of combining stochastic volatility, jump risk, and discrete sampling in a unified pricing methodology.

The stochastic-volatility component of the present paper is rooted in the classical Heston model, in which the asset return and its instantaneous variance are driven by correlated Brownian motions and the variance follows a mean-reverting square-root diffusion [18]. This structure provides a tractable explanation for volatility smiles and term structures while preserving transform-based pricing. The introduction of finite-activity price jumps leads to the Bates-type stochastic-volatility jump-diffusion framework [3], which is particularly relevant for variance swap valuation because jumps enter realized quadratic variation directly. More generally, affine jump-diffusion models show that stochastic volatility and jump risk can be incorporated into derivative pricing through Riccati equations and exponential-affine transforms [9]. Related Fourier-transform and Levy-jump specifications, such as the tempered-stable jump model of Zaevski et al. [29], further illustrate how jump tails and stochastic volatility can be combined in option valuation. The present model belongs to this affine-transform tradition, but it modifies the variance mean-reversion target by adding a persistent macro-liquidity state variable.

A closely related line of research studies jump-diffusion and regime-dependent structures in derivative pricing. In incomplete markets with regime changes, Elliott et al. [10] analyze option pricing under a generalized Markov-modulated jump-diffusion model and derive the corresponding partial integro-differential equation(PIDE) system under an equivalent martingale measure. Their work illustrates how regime switches and jumps can be jointly incorporated into derivative valuation. In a different derivative setting, Wang et al. [24] study power exchange options with counterparty risk and jump risk, showing that both idiosyncratic and common jumps induced by information arrivals can substantially affect option values. In commodity and futures markets, Ewald and Zou [11] obtain analytic formulas for futures and options under a linear-quadratic jump-diffusion model with seasonal stochastic volatility and convenience yield, while Hu et al. [19] examine equilibrium pricing of European crude oil options under stochastic behavior and jump risks. These studies indicate that jump risk is an economically meaningful channel through which extreme price movements enter derivative prices. This view is also supported by empirical evidence in Bégin et al. [4], who document that idiosyncratic jump risk plays a central role in explaining option-implied risk premia.

Another important development concerns stochastic long-run variance or stochastic equilibrium levels in Heston-type models. The classical Heston model assumes a constant long-run variance mean, but this assumption is often too restrictive for explaining the term structure of implied volatility and variance swap curves. To address this limitation, He and Chen [14] introduce a stochastic long-term mean into a Heston-type stochastic volatility model and derive a closed-form pricing formula for European options, preserving the analytical tractability of the original Heston framework. Yoon et al. [28] further derive closed-form variance swap pricing formulas under Heston models with stochastic long-run mean of variance, showing that such specifications can better capture unstable market conditions. For volatility derivatives, He and Lin [15] obtain an analytical forward characteristic function and pricing formula for discretely sampled volatility swaps under a modified risk-neutralized Heston model with a stochastic long-run variance level. Extending this direction, Fu [13] studies variance swaps under a Heston model with stochastic long-run mean and jumps, deriving the joint moment-generating function, discretely sampled variance swap formula, and continuously sampled limiting formula through a Feynman–Kac PIDE approach. More recently, He and Lin [16] incorporate stochastic volatility, stochastic equilibrium levels, and regime switching into the valuation of variance and volatility swaps. These studies collectively show that the long-run variance target should be treated as an active state variable rather than as a fixed parameter.

In parallel, a large literature has emphasized the role of liquidity risk in asset pricing and derivative valuation. Early empirical evidence in Brenner et al. [5] shows that illiquidity can significantly reduce option values when options are nontradable or subject to market frictions. At the asset-pricing level, Pástor and Stambaugh [23] demonstrate that aggregate liquidity is a priced state variable, while Keene and Peterson [20] show that liquidity remains an important factor in explaining portfolio returns even after controlling for standard risk factors. From a portfolio selection perspective, Abensur et al. [1] construct a stochastic liquidity model and show its usefulness in investment portfolio formation. These contributions provide the economic motivation for treating liquidity not as a secondary market imperfection, but as a persistent state variable that can affect expected returns, risk premia, and derivative prices.

Recent financial-system applications in computational economics also emphasize the usefulness of formal quantitative frameworks for financial efficiency assessment and uncertain portfolio decisions. For example, Mesgarani et al. [21] propose a fuzzy-based efficiency assessment method for financial systems, while Wu et al. [26] study portfolio optimization under an uncertain financial model. These studies are not variance swap pricing models, but they illustrate the broader use of formal quantitative methods in financial-system assessment and uncertain financial decision-making.

The incorporation of stochastic liquidity into derivative pricing has also received increasing attention. Feng et al. [12] develop a liquidity-adjusted option pricing model in which stochastic market liquidity affects stock prices through a liquidity discount factor, and their empirical results support the importance of liquidity risk for option pricing, especially for out-of-the-money and longer-maturity contracts. Xu et al. [27] extend this idea to variance and volatility swaps by deriving pricing formulas under a liquidity-adjusted underlying asset model with stochastic liquidity risk. Pasricha and He [22] examine exchange options with stochastic liquidity risk and derive a closed-form pricing formula without requiring a change of numeraire. Wang et al. [25] further study generalized variance swaps under a jump-diffusion model with stochastic liquidity risk and obtain the pricing formula through the joint moment-generating function generated by solving the associated PIDE. In the context of American options, Zhang et al. [30] incorporate both stochastic liquidity risk and jump risk and use the Fourier-cosine series expansion

(COS) method together with Richardson extrapolation to obtain analytical approximation formulas. More recently, He and Lin [17] propose a stochastic liquidity risk model with stochastic volatility for European option pricing, while Chen et al. [7] introduce stochastic liquidity risks into commodity futures option pricing under commodity financialization. These studies confirm that stochastic liquidity is an economically relevant and analytically tractable factor in derivative pricing.

The distinction from the existing literature is therefore precise. In Heston and Bates-type models, the long-run variance target is typically constant. In stochastic-long-run-mean extensions, the target is stochastic but largely latent. In liquidity-adjusted derivative models, liquidity usually affects the asset-price process, the discount channel, or a direct liquidity-adjustment term. By contrast, this paper places macro-liquidity in the variance mean-reversion target itself. This creates a direct and economically interpretable channel from persistent financial conditions to future expected quadratic variation, which is the object priced by a variance swap.

This paper is positioned at the intersection of these strands of literature. Following the transform-based variance swap pricing tradition of Zhu and Lian [31], Broadie and Jain [6], Cui et al. [8], and Fu [13], we derive analytical pricing formulas for discretely and continuously sampled variance swaps under a jump-diffusion stochastic volatility model. Building on the stochastic long-run variance literature represented by He and Chen [14], Yoon et al. [28], He and Lin [15] and He and Lin [16], we retain a stochastic variance target rather than a constant Heston mean. At the same time, motivated by the liquidity-risk evidence and models in Pástor and Stambaugh [23], Keene and Peterson [20], Feng et al. [12], Xu et al. [27], Wang et al. [25], and related studies, we introduce an exogenous macro-liquidity state variable into the variance mean-reversion target. Specifically, the instantaneous variance reverts to the effective target

$$\theta_t + \alpha_y y_t, \tag{1.1}$$

where θ_t represents the latent stochastic long-run variance component and y_t captures persistent macro-liquidity or market-stress conditions. This specification provides a direct channel through which observable low-frequency financial conditions affect future expected variance while preserving the exponential-affine transform structure needed for tractable variance swap valuation.

Mathematically, the pricing problem can be formulated through the backward partial integro-differential equation associated with the jump-diffusion generator. Existing studies have used partial differential equation (PDE)/PIDE methods, Fourier-transform techniques, affine Riccati systems, numerical quadrature, Monte Carlo simulation, and COS-type expansions to evaluate options and realized-variance derivatives under stochastic volatility and jumps. The contribution of the present paper is to show that the additional macro-liquidity-to-variance-target channel preserves the affine structure while adding a linear Riccati equation and an additional quadratic term in the transform coefficient.

The paper makes four contributions. First, it introduces a macro-liquidity-to-variance-target channel that links persistent liquidity or market-stress conditions directly to the future path of spot variance. Second, it derives the exponential-affine transform, the Riccati representation, the discretely sampled actual-return variance swap strike, and the continuous-monitoring limiting strike in a unified framework. Third, it establishes finite-horizon transform admissibility conditions and proves the convergence of the discrete actual-return strike to the continuous quadratic-variation benchmark. Fourth, it quantifies the pricing effect of the macro-liquidity channel through nested-model comparisons, strike decomposition, Monte Carlo validation, and robustness checks.

2. Model dynamics

All pricing results are derived under a risk-neutral probability measure $\mathbb{Q}$ on a filtered probability space $(\Omega, \mathcal{F}, \{\mathcal{F}_t\}_{t\geq 0}, \mathbb{Q})$. The process S_t denotes the ex-dividend price of the underlying asset, $x_t = \ln S_t$ denotes its log-price, v_t is the instantaneous variance, θ_t is the stochastic long-run variance component, and y_t is a persistent macro-liquidity or market-stress state variable. The macro-liquidity state affects the model through the effective variance target $\theta_t + \alpha_y y_t$.

The risk-neutral dynamics are specified as follows:

$$\begin{cases} \dfrac{dS_t}{S_t} = (r - d - \lambda m)dt + \sqrt{v_t}dW_t^S + (e^{J^S} - 1)dN_t, \\ dv_t = \kappa_v(\theta_t + \alpha_y y_t - v_t)dt + \sigma_v \sqrt{v_t}dW_t^v + J^v dN_t, \\ d\theta_t = \kappa_\theta(\bar{\theta} - \theta_t)dt + \sigma_\theta dW_t^\theta, \\ dy_t = \kappa_y(\bar{y} - y_t)dt + \sigma_y dW_t^y. \end{cases} \tag{2.1}$$

The parameters r and d denote the risk-free rate and continuous dividend yield, respectively. The constants κ_v and σ_v are the mean-reversion speed and volatility-of-volatility of v_t, respectively. The parameters κ_θ, $\bar{\theta}$, and σ_θ govern the stochastic long-run variance component θ_t. The parameters κ_y, $\bar{y}$, and σ_y govern the macro-liquidity factor y_t. The coefficient α_y measures the strength and sign of the macro-liquidity feedback into the variance target. The jump parameters $\lambda, \eta, \mu_J, \rho_J$ and δ_J describe the jump arrival intensity, the mean variance-jump size, the conditional mean of the price jump, the price-variance jump loading, and the conditional price-jump volatility, respectively.

The Brownian motions W^S, W^v, W^θ, and W^y are standard Brownian motions under $\mathbb{Q}$. We assume $d\langle W^S, W^v\rangle_t = \rho_{sv}dt$, while W^θ and W^y are independent of (W^S, W^v). The Poisson process N_t has constant intensity λ and is independent of the Brownian motions. The jump-size sequence $\{(J_i^S, J_i^v)\}_{i\geq 1}$ is i.i.d., independent of N_t and of the Brownian part.

The same Poisson counter is used in the asset-price and variance equations intentionally. This specification represents common price-variance jump arrivals: when a market-wide shock occurs, the asset price may jump and the variance may jump at the same event time. This is consistent with stochastic-volatility jump models in which discontinuous price movements and sudden variance shocks are jointly triggered by rare information arrivals.

The variance-jump and price-jump sizes satisfy

$$J^v \sim \mathrm{Exp}(1/\eta), \qquad J^S \mid J^v \sim N(\mu_J + \rho_J J^v, \delta_J^2). \tag{2.2}$$

The compensator is

$$m = \mathbb{E}^{\mathbb{Q}}[e^{J^S} - 1] = \frac{\exp(\mu_J + \delta_J^2/2)}{1 - \rho_J\eta} - 1, \tag{2.3}$$

provided $1 - \rho_J\eta > 0$.

Remark 1 (Risk-neutral specification)**.** The model is stated directly under the risk-neutral measure $\mathbb{Q}$, because the objective of this paper is variance swap valuation rather than the econometric identification of physical risk premia. The parameters $\kappa_y, \bar{y}$ and σ_y should therefore be interpreted as risk-neutral macro-liquidity parameters. If one starts from a physical liquidity process, an affine market price of liquidity risk can preserve the Ornstein–Uhlenbeck form under an equivalent martingale measure. A complete change of measure for all Brownian and jump components is not required for the pricing formulas derived below and is left for empirical calibration work.

The variance process has the same square-root diffusion coefficient as the Heston model but a stochastic target $\theta_t + \alpha_y y_t$. The next section states the finite-horizon transform domain on which the affine pricing formulas are used.

3. Joint moment-generating function

The log-price $x_t = \ln S_t$ has already been introduced in Section 2. In this section, lower-case symbols without time subscripts denote state arguments, while time-subscripted symbols denote stochastic processes. To avoid confusing the state argument with the process θ_t, we write the generic state of the long-run variance component as ϑ. The joint moment-generating function (MGF) of x_T, v_T, θ_T, and y_T under $\mathbb{Q}$ is defined by

$$U(\tau, x, v, \vartheta, y; \phi, b, c, f, \gamma) = \mathbb{E}^{\mathbb{Q}}[\exp(\phi x_T + b v_T + c\theta_T + f y_T + \gamma) \mid x_t = x,\ v_t = v,\ \theta_t = \vartheta,\ y_t = y] \,. \tag{3.1}$$

Let $\tau = T - t$ be the time to maturity and let $\mathbf{q} = (\phi, b, c, f, \gamma)^\top$, where ϕ, b, c, f and γ are real constants. The closed-form expression for this joint MGF is given in the lemma below.

Lemma 1 (Joint moment-generating function)**.** *Assume the underlying asset price follows the dynamics specified in Eq* (2.1)*. Then, the joint MGF $U(\tau, x, v, \vartheta, y; \phi, b, c, f, \gamma)$ takes the exponential-affine form*

$$U(\tau, x, v, \vartheta, y; \phi, b, c, f, \gamma) = \exp(\phi x + B(\tau)v + C(\tau)\vartheta + F(\tau)y + D(\tau) + E(\tau)) \,. \tag{3.2}$$

where

$$A = \kappa_v - \rho_{sv}\sigma_v\phi, \qquad \delta_1 = \sqrt{A^2 + \sigma_v^2(\phi - \phi^2)}, \qquad \delta_2 = \frac{A - b\sigma_v^2}{\delta_1}, \tag{3.3}$$

$$B(\tau) = \frac{1}{\sigma_v^2}\left[A - \delta_1 \frac{\sinh(\delta_1\tau/2) + \delta_2\cosh(\delta_1\tau/2)}{\cosh(\delta_1\tau/2) + \delta_2\sinh(\delta_1\tau/2)}\right], \tag{3.4}$$

$$C(\tau) = ce^{-\kappa_\theta\tau} + \kappa_v e^{-\kappa_\theta\tau}\int_0^\tau e^{\kappa_\theta s}B(s)ds, \tag{3.5}$$

$$F(\tau) = fe^{-\kappa_y\tau} + \alpha_y\kappa_v e^{-\kappa_y\tau}\int_0^\tau e^{\kappa_y s}B(s)ds, \tag{3.6}$$

$$D(\tau) = \gamma + \int_0^\tau \left[(r-d)\phi + \kappa_\theta\bar{\theta}C(s) + \kappa_y\bar{y}F(s) + \frac{1}{2}\sigma_\theta^2 C(s)^2 + \frac{1}{2}\sigma_y^2 F(s)^2\right] ds, \tag{3.7}$$

$$E(\tau) = \int_0^\tau \lambda\left(\frac{\exp(\phi\mu_J + \phi^2\delta_J^2/2)}{1 - \eta(B(s) + \phi\rho_J)} - 1 - m\phi\right) ds. \tag{3.8}$$

Proof. The result follows from applying the Feynman–Kac PIDE to the four-factor affine jump-diffusion state vector and substituting the exponential-affine ansatz. Matching the coefficients of the state variables gives the Riccati system, and the jump term is evaluated by the conditional exponential transform of J^S and J^v. Solving the scalar Riccati equation for B, followed by the linear equations for C and F and the integral equations for D and E, gives the stated formula. The detailed proof is given in A.1.□

Proposition 1 (Finite-horizon transform admissibility)**.** *Fix a finite horizon T and a monitoring interval $\Delta \le T$. For $p \in \{1,2\}$, let $B_p(s)$ denote the Riccati B-coefficient in Lemma 1 initialized at $(\phi, b, c, f, \gamma) = (p, 0, 0, 0, 0)$, and let $\widehat{B}_p(s;\Delta)$ denote the Riccati B-coefficient used in the second tower-property step, initialized at $(\phi, b, c, f, \gamma) = (0, B_p^\Delta, C_p^\Delta, F_p^\Delta, 0)$. Suppose that the jump-transform denominators satisfy*

$$1 - \rho_J \eta > 0, \qquad 1 - 2\rho_J \eta > 0, \tag{3.9}$$

$$1 - \eta\big(B_p(s) + p\rho_J\big) > 0, \qquad 0 \le s \le T, \quad p = 1, 2, \tag{3.10}$$

and, for the second transform,

$$1 - \eta \widehat{B}_p(s;\Delta) > 0, \qquad 0 \le s \le T, \quad p = 1, 2. \tag{3.11}$$

Assume further that the explicit Riccati denominator does not vanish along the relevant trajectories; in particular,

$$\cosh(\delta_{1,p}s/2) + \delta_{2,p}\sinh(\delta_{1,p}s/2) \neq 0, \qquad 0 \le s \le T, \quad p = 1, 2, \tag{3.12}$$

and the analogous denominator for the hatted Riccati trajectories is also nonzero on $[0, T]$*. Then, the exponential-affine transforms used in Lemma 1 and Theorem 1 are finite on the required time intervals. Consequently, the discretely sampled actual-return variance swap strike in* (4.6) *is well defined under the stated moment restrictions.*

Proof. The admissibility restrictions exclude the finite-horizon singularities relevant for the affine transforms used in the discrete strike formula. The Riccati trajectory must remain finite, and the exponential jump transform must remain inside its moment domain. The first set of restrictions applies to the one-step transforms with $p = 1, 2$, while the second set applies to the tower-property transform with $\phi = 0$. The detailed proof is given in A.2. This admissibility statement is deliberately finite-horizon. Because θ_t and y_t are Gaussian OU factors, the target $\theta_t + \alpha_y y_t$ is not globally constrained to be positive. Consequently, the classical CIR Feller condition alone does not ensure strict positivity of v_t in the original affine specification. The pricing formulas are interpreted on the finite-horizon transform domain specified above, while the Monte Carlo implementation uses full truncation to maintain numerical non-negativity of the simulated variance paths.□

4. Discretely sampled variance swaps

Before defining the fair strike, note that the time-zero value of a variance swap with maturity payoff $RV_T - K$ is

$$V_0 = e^{-rT}\mathbb{E}^{\mathbb{Q}}[RV_T - K]. \tag{4.1}$$

Since both the realized-variance leg and the fixed leg are paid at maturity and the interest rate is deterministic in the present model, the discount factor cancels from the zero-value condition $V_0 = 0$. Hence, the fair strike is $K = \mathbb{E}^{\mathbb{Q}}[RV_T]$. The formulas below therefore report fair strikes rather than time-zero present values.

Consider a discrete set of sampling dates $t_i = iT/N$ for $i = 0, 1, \ldots, N$, where $T > 0$ is the maturity and $N \in \mathbb{N}$ is the number of sampling points. The fair strike of a variance swap based on the actual return over these discrete intervals is given under the risk-neutral measure $\mathbb{Q}$ by

$$K_{\mathrm{var}}^{(1)}(N) = \frac{100^2}{T}\sum_{i=1}^{N}\mathbb{E}^{\mathbb{Q}}\left[\left(\frac{S_{t_i}-S_{t_{i-1}}}{S_{t_{i-1}}}\right)^2\right], \tag{4.2}$$

where S_t denotes the price of the underlying asset. Setting $\Delta = T/N$ and writing $S_t = e^{x_t}$, we obtain

$$\left(\frac{S_{t_i}-S_{t_{i-1}}}{S_{t_{i-1}}}\right)^2 = e^{2(x_{t_i}-x_{t_{i-1}})} - 2e^{x_{t_i}-x_{t_{i-1}}} + 1. \tag{4.3}$$

Based on the above decomposition, we derive the explicit closed-form pricing formula for the discrete variance swap strike in the following theorem.

Theorem 1. *Let $\Delta = T/N$ and for $p \in \{1,2\}$ denote by $B_p^{\Delta}, C_p^{\Delta}, F_p^{\Delta}, D_p^{\Delta}, E_p^{\Delta}$ the Riccati coefficients of Lemma 1 evaluated at time Δ with initial vector $(\phi, b, c, f, \gamma) = (p, 0, 0, 0, 0)$. For $t \geq 0$ let*

$$\widehat{B}_p(t;\Delta),\ \widehat{C}_p(t;\Delta),\ \widehat{F}_p(t;\Delta),\ \widehat{D}_p(t;\Delta),\ \widehat{E}_p(t;\Delta) \tag{4.4}$$

be the Riccati coefficients of Lemma 1 evaluated at time t with initial vector $(\phi, b, c, f, \gamma) = (0, B_p^{\Delta}, C_p^{\Delta}, F_p^{\Delta}, 0)$. Define

$$\begin{aligned}\mathcal{M}_p(t;\Delta) = \exp\Big(&D_p^{\Delta} + E_p^{\Delta} + \widehat{B}_p(t;\Delta)v_0 + \widehat{C}_p(t;\Delta)\theta_0 + \widehat{F}_p(t;\Delta)y_0 \\ &+ \widehat{D}_p(t;\Delta) + \widehat{E}_p(t;\Delta)\Big).\end{aligned} \tag{4.5}$$

Then, the discretely sampled actual-return variance swap strike is

$$K_{\mathrm{var}}^{(1)}(N) = \frac{100^2}{T}\sum_{i=1}^{N}\Big[\mathcal{M}_2(t_{i-1};\Delta) - 2\mathcal{M}_1(t_{i-1};\Delta) + 1\Big]. \tag{4.6}$$

Proof. The squared actual return is decomposed into two conditional exponential moments of log-price increments. Lemma 1 evaluates the first conditional transform over one monitoring interval, and the tower property evaluates the remaining expectation over the state vector at the previous monitoring date. Summing over all monitoring intervals yields the stated discrete actual-return variance swap strike. The detailed proof is given in A.3.□

5. Continuous-time limit of discretely sampled variance swaps

We now turn to the pricing of variance swaps under continuous monitoring. The continuously sampled realized variance provides a theoretical benchmark, and its expectation under the risk-neutral measure can be obtained explicitly within our affine framework. For an asset price process S_t with stochastic volatility and jumps, the continuously sampled realized variance over $[0, T]$ is defined as

$$RV_T^c = \frac{100^2}{T}\left(\int_0^T v_t\,dt + \sum_{i=1}^{N_T}(e^{J_i^S} - 1)^2\right), \tag{5.1}$$

where v_t is the instantaneous variance, N_T is a Poisson process with intensity λ, and J_i^S are the log-price jumps. The fair strike of a continuously sampled variance swap is then $K_{\text{var}}^c = \mathbb{E}^{\mathbb{Q}}[RV_T^c]$. As in the discrete case, the deterministic discount factor cancels in the zero-value fair-strike condition. The following theorem provides a closed-form expression for K_{var}^c under the model assumptions detailed in previous sections.

Theorem 2 (Continuously sampled variance swap strike). *Assume $\kappa_v \neq \kappa_\theta$ and $\kappa_v \neq \kappa_y$; the coincident-rate cases are obtained by continuous limits. Define*

$$\bar{v}_\infty = \bar{\theta} + \alpha_y \bar{y} + \frac{\lambda\eta}{\kappa_v}, \tag{5.2}$$

and

$$J_2 = \frac{e^{2\mu_J + 2\delta_J^2}}{1 - 2\rho_J\eta} - \frac{2e^{\mu_J + \delta_J^2/2}}{1 - \rho_J\eta} + 1. \tag{5.3}$$

Then, the continuously sampled variance swap fair strike is

$$\begin{aligned} K_{\text{var}}^c = \frac{100^2}{T}\Bigg[& \bar{v}_\infty T + (v_0 - \bar{v}_\infty)\frac{1 - e^{-\kappa_v T}}{\kappa_v} \\ & + \frac{\kappa_v(\theta_0 - \bar{\theta})}{\kappa_v - \kappa_\theta}\left(\frac{1 - e^{-\kappa_\theta T}}{\kappa_\theta} - \frac{1 - e^{-\kappa_v T}}{\kappa_v}\right) \\ & + \frac{\kappa_v \alpha_y (y_0 - \bar{y})}{\kappa_v - \kappa_y}\left(\frac{1 - e^{-\kappa_y T}}{\kappa_y} - \frac{1 - e^{-\kappa_v T}}{\kappa_v}\right) + \lambda T J_2 \Bigg]. \end{aligned} \tag{5.4}$$

Proof. The continuous-monitoring strike is the expectation of integrated variance plus the expected jump quadratic-variation contribution. The conditional means of θ_t and y_t are obtained from their Ornstein–Uhlenbeck dynamics, and the mean of v_t follows a linear inhomogeneous ordinary differential equation (ODE). Integrating this mean path and adding the second jump moment gives the closed-form continuous-monitoring strike. The detailed proof is given in A.4.□

The discrete actual-return strike derived in Section 4 (for equally spaced monitoring) converges to the continuously sampled strike as the monitoring mesh vanishes. The following theorem generalises this convergence to arbitrary deterministic sampling schemes, thereby justifying the continuous-time formula as the limit of discretely monitored variance swaps.

Theorem 3 (Convergence from discrete to continuous sampling). *Let $\Pi_N = \{0 = t_0 < t_1 < \cdots < t_N = T\}$ be a deterministic partition of $[0, T]$ with mesh $|\Pi_N| = \max_i(t_i - t_{i-1})$. Under the moment-domain restrictions stated in Lemma 1 and with finite jump intensity $\lambda < \infty$, the discretely sampled actual-return variance swap strike satisfies*

$$\lim_{|\Pi_N| \to 0} K_{\text{var}}^{(1)}(\Pi_N) = K_{\text{var}}^c, \tag{5.5}$$

where $K_{\text{var}}^{(1)}(\Pi_N)$ denotes the fair strike defined in (4.2) (with t_i taken from Π_N).

Proof. The discrete actual-return realized variance is compared with the quadratic variation of the relative price return semimartingale. On jump-free intervals, the difference between simple returns and stochastic-integral increments is of smaller order than the mesh. On jump intervals, finite activity ensures that isolated jumps contribute $(e^{J^S} - 1)^2$ in the limit. Uniform integrability under the stated moment restrictions upgrades convergence in probability to convergence of expectations. The detailed proof is given in A.5. □

Thus, the continuous-time strike K^c_{var} serves both as a practical approximation for daily or weekly monitoring and as a theoretical limit that links the discrete pricing formula to the underlying continuous semimartingale properties of the asset.

6. Numerical experiments

The numerical design uses the two parameter samples reported in Fu [13], the same values (i.e., $r = 0.01$, $T = 1$, $\lambda = 0.2$, $\eta = 0.05$, $\mu_J = 0.01$, $\rho_J = -0.086$, and $\delta_J = 0.02$), and the same tabulated frequencies (i.e., monthly $N = 12$, fortnightly $N = 26$, weekly $N = 52$, and daily $N = 252$). To make the Monte Carlo validation visually more informative, Figure 1 reports relative discrepancies over 20 values of N between 12 and 252. The sensitivity experiments in Figures 2 and 3 also use 20 grid points for each varied parameter. The new parameters are α_y, y_0, $\bar{y}$, κ_y, and σ_y. They are small enough to preserve stable positive variance dynamics under full truncation and large enough to visibly affect the fair strike.

To verify that the augmented model nests the relevant earlier specifications, we also conduct two reference-model reduction checks. The common stochastic-variance parameter sets used in these checks are reported in Table 1; these are the sample values used in Fu [13] for the Heston model with stochastic long-run mean of variance and jumps.

Table 1. Benchmark parameter sets used in the numerical experiments and reduction checks.

Market and variance block			Jump-risk and macro-liquidity block		
Parameter	Sample 1	Sample 2	Parameter	Sample 1	Sample 2
Market and contract parameters			*Jump-risk parameters*		
r	0.0100	0.0100	λ	0.2000	0.2000
d	0.0000	0.0000	η	0.0500	0.0500
T	1.0000	1.0000	μ_J	0.0100	0.0100
			ρ_J	−0.0860	−0.0860
			δ_J	0.0200	0.0200
Variance and long-run mean parameters			*Macro-liquidity parameters*		
κ_v	5.0000	6.3000	α_y	0.0800	0.0700
v_0	0.1000	0.1600	y_0	0.0400	0.0500
θ_0	0.1500	0.1100	$\bar{y}$	0.0300	0.0350
$\bar{\theta}$	0.1000	0.1250	κ_y	2.2000	2.6000
σ_v	0.0050	0.0120	σ_y	0.0150	0.0120
κ_θ	4.0000	3.6000			
σ_θ	0.0100	0.0040			
ρ_{sv}	−0.5000	−0.7000			

Note. The reference-model reduction checks use the same variance and long-run mean parameters reported in this table. The Fu-type reduction sets the macro-liquidity channel to zero, while the Yoon-type reduction additionally removes the jump channel, as described in the text.

Table 1 reports the two benchmark parameter sets used in the numerical experiment. Sample 2 has a larger initial variance v_0, faster variance mean reversion κ_v, and a more negative return-variance correlation ρ_{sv} than Sample 1, while the jump parameters are kept fixed across the two samples. This design separates the effect of the stochastic variance block from the common jump-risk channel.

6.1. Comparison with existing literature

First, setting $\alpha_y = \kappa_y = \sigma_y = 0$ removes the macro-liquidity channel and reduces the model to Fu [13], *Analytic solutions of variance swaps for Heston models with stochastic long-run mean of variance and jumps*. In the tables, AS denotes the affine or semi-analytical strike, CON denotes the continuous-monitoring strike, MC denotes the Monte Carlo estimate, and RD denotes the relative discrepancy. Table 2 compares the analytic discrete strike and the continuous strike produced by the present implementation with the reported values in Fu [13]. The agreement is exact up to numerical rounding, confirming that the additional macro-liquidity state preserves the underlying affine-transform structure as a conservative extension of the jump model.

Table 2. Reduction to [13] when $\alpha_y = \kappa_y = \sigma_y = 0$.

Sample	Frequency	This paper AS	Fu AS	Abs. diff.	This paper CON	Fu CON
Sample 1	Monthly ($N = 12$)	1141.0764	1141.0764	0.0000	1133.8657	1133.8657
Sample 1	Fortnightly ($N = 26$)	1137.1822	1137.1822	0.0000	1133.8657	1133.8657
Sample 1	Weekly ($N = 52$)	1135.5213	1135.5212	0.0001	1133.8657	1133.8657
Sample 1	Daily ($N = 252$)	1134.2069	1134.2058	0.0011	1133.8657	1133.8657
Sample 2	Monthly ($N = 12$)	1288.9977	1288.9977	0.0000	1280.6165	1280.6165
Sample 2	Fortnightly ($N = 26$)	1284.4478	1284.4478	0.0000	1280.6165	1280.6165
Sample 2	Weekly ($N = 52$)	1282.5236	1282.5236	0.0000	1280.6165	1280.6165
Sample 2	Daily ($N = 252$)	1281.0086	1281.0086	0.0000	1280.6165	1280.6165

Second, setting $\alpha_y = \kappa_y = \sigma_y = \lambda = 0$ removes both the macro-liquidity channel and the jump channel, giving the stochastic-long-run-mean Heston model considered by Yoon et al. [28]. Table 3 compares the resulting discrete actual-return strikes with the Yoon-formula values reported in Fu [13]. This difference reflects the different realized-variance definitions used in the two formulas: Yoon et al. [28] use logarithmic returns, whereas this paper prices variance swaps based on actual returns. Therefore, Table 3 should be read as a definition-sensitive comparison.

Table 3. Reduction to [28] when $\alpha_y = \kappa_y = \sigma_y = \lambda = 0$.

Sample	Frequency	This paper	Yoon formula	Abs. diff.
Sample 1	Monthly ($N = 12$)	1123.9016	953.1450	170.7566
Sample 1	Weekly ($N = 52$)	1118.5232	950.8380	167.6852
Sample 1	Daily ($N = 252$)	1117.2517	950.2480	167.0037
Sample 2	Monthly ($N = 12$)	1274.5175	1272.5100	2.0075
Sample 2	Weekly ($N = 52$)	1268.2004	1267.8800	0.3204
Sample 2	Daily ($N = 252$)	1266.7234	1266.6700	0.0534

6.2. Monte Carlo simulation

The Monte Carlo simulation uses a full-truncation Euler scheme on the monitoring grid. Let $\Delta t = T/N$, $v_n^+ = \max(v_n, 0)$, and let $Z_n^S, Z_n^\perp, Z_n^\theta, Z_n^y$ be independent standard normals. Set

$$Z_n^v = \rho_{sv} Z_n^S + \sqrt{1-\rho_{sv}^2}\, Z_n^\perp. \tag{6.1}$$

If $K_n \sim \text{Poisson}(\lambda\Delta t)$ is the number of jumps in $(t_n, t_{n+1}]$, define

$$\Delta J_n^v = \sum_{k=1}^{K_n} J_{n,k}^v, \qquad \Delta J_n^S = \sum_{k=1}^{K_n} J_{n,k}^S. \tag{6.2}$$

The simulated states are updated by

$$\begin{cases} x_{n+1} = x_n + \left(r - d - \lambda m - \dfrac{1}{2} v_n^+\right)\Delta t + \sqrt{v_n^+}\sqrt{\Delta t}\, Z_n^S + \Delta J_n^S, \\ v_{n+1} = \max\left\{v_n + \kappa_v(\theta_n + \alpha_y y_n - v_n^+)\Delta t + \sigma_v \sqrt{v_n^+}\sqrt{\Delta t}\, Z_n^v + \Delta J_n^v, 0\right\}, \\ \theta_{n+1} = \theta_n + \kappa_\theta(\bar{\theta} - \theta_n)\Delta t + \sigma_\theta \sqrt{\Delta t}\, Z_n^\theta, \\ y_{n+1} = y_n + \kappa_y(\bar{y} - y_n)\Delta t + \sigma_y \sqrt{\Delta t}\, Z_n^y. \end{cases} \tag{6.3}$$

Table 4 shows a clean convergence pattern. For Sample 1, the analytic discrete strike decreases from 1163.4906 at monthly sampling to 1156.3870 at daily sampling, approaching the continuous strike 1156.0341. The same monotone pattern appears in Sample 2, where the analytic strike decreases from 1313.4335 to 1305.1731 and approaches the continuous strike 1304.7677. This behavior is economically natural. Coarser actual-return sampling captures compounding and jump-amplified return effects over longer intervals, whereas finer sampling makes the realized variance closer to instantaneous quadratic variation.

Table 4. Fair strike prices under the macro-liquidity augmented model.

Sample	Frequency	AS	MC	CON	SE	RD(%)
Sample 1	Monthly ($N = 12$)	1163.4906	1171.6352	1156.0341	2.9318	0.7000
Sample 1	Fortnightly ($N = 26$)	1159.4636	1161.7649	1156.0341	1.9325	0.1985
Sample 1	Weekly ($N = 52$)	1157.7462	1159.8196	1156.0341	1.3768	0.1791
Sample 1	Daily ($N = 252$)	1156.3870	1157.6178	1156.0341	0.6790	0.1064
Sample 2	Monthly ($N = 12$)	1313.4335	1311.1821	1304.7677	3.2562	-0.1714
Sample 2	Fortnightly ($N = 26$)	1308.7292	1307.8183	1304.7677	2.1525	-0.0696
Sample 2	Weekly ($N = 52$)	1306.7397	1305.0643	1304.7677	1.5182	-0.1282
Sample 2	Daily ($N = 252$)	1305.1731	1305.2961	1304.7677	0.7282	0.0094

The Monte Carlo estimates provide numerical support for the affine pricing implementation. The relative discrepancy RD is 0.7000% for the coarsest Sample 1 case and remains close to zero at the finer frequencies. In Sample 2, the relative discrepancy ranges from −0.1714% at monthly sampling to 0.0094% at daily sampling. Since all absolute relative errors are far below the 2% rejection threshold, the evidence supports both the Riccati implementation and the jump simulation mechanism. The standard errors also decline as sampling frequency increases because each path's realized variance becomes less exposed to a small number of coarse interval returns.

The comparison between Sample 1 and Sample 2 is informative. Sample 2 has a larger initial variance $v_0 = 0.16$, a larger variance mean-reversion speed $\kappa_v = 6.3$, and a more negative return-variance correlation $\rho_{sv} = -0.7$. Its fair strikes are therefore consistently higher than those of Sample 1. The macro-liquidity factor adds another persistent contribution through $\alpha_y y_t$, raising the effective target of v_t by approximately $\alpha_y \bar{y}$ in the long run. This explains why the augmented model's strikes are above the corresponding reference-paper levels: the extension changes the expected integrated variance path and therefore has a direct pricing implication.

Figure 1 refines the validation diagnosis by using 20 sampling frequencies in addition to the four frequencies reported in the table. The plotted statistic is the relative discrepancy $(MC - AS)/AS$, so the horizontal zero line represents exact agreement between Monte Carlo and the affine-transform price. For both samples the points fluctuate around zero and remain inside the ±2% band, with no visible frequency-dependent bias. This diagnostic shows that changing the monitoring frequency alters the strike level without creating a systematic pricing error relative to the analytic transform.

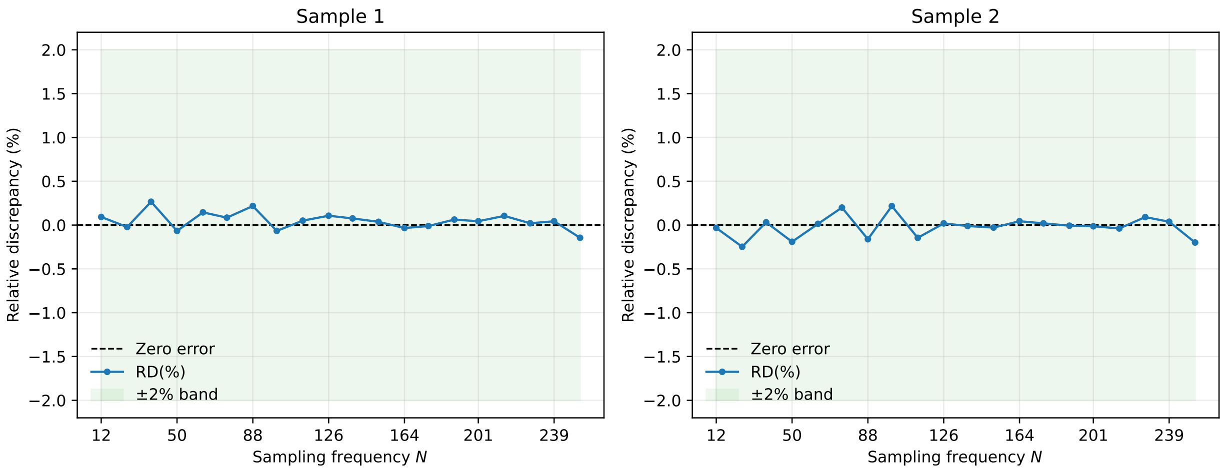

Figure 1. Relative Monte Carlo discrepancy $(MC - AS)/AS$ over 20 sampling-frequency points. The shaded band marks the ±2% validation threshold.

6.3. *Parameter sensitivity analysis*

Figure 2 uses 20 values for each stochastic long-run mean parameter, which makes the local slope and curvature more visible than a sparse grid. The κ_θ panel shows the economics of mean-reversion speed. In Sample 2, $\bar{\theta} = 0.125$ is above $\theta_0 = 0.11$, so a larger κ_θ pulls θ_t upward more rapidly, raises the expected future variance target, and increases the variance swap strike. The $\bar{\theta}$ and θ_0 panels are close to linear because they shift the conditional mean path of the variance target directly. A higher $\bar{\theta}$ raises the long-horizon anchor, whereas a higher θ_0 raises the short- and medium-horizon target immediately. The σ_θ panel is economically different: volatility of the long-run mean does not raise $\mathbb{E}[\theta_t]$ directly, but it raises the transform through convexity, especially through the $\sigma_\theta^2 C(\tau)^2/2$ term in D'. Thus, its impact should be read as a convexity premium for uncertainty about the future variance target rather than as a level effect.

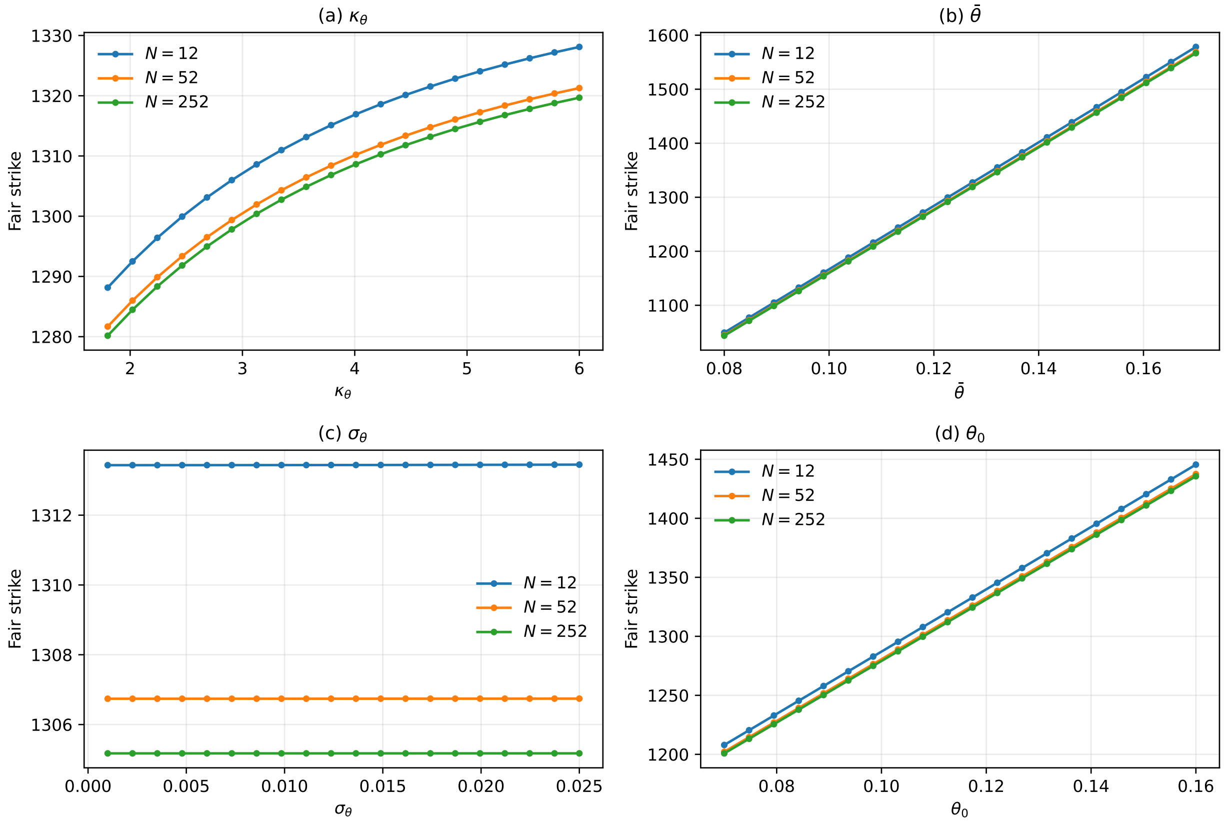

Figure 2. Sensitivity of the analytic fair strike to stochastic long-run variance parameters on 20-point parameter grids. Panel (a): κ_θ; Panel (b): $\bar{\theta}$; Panel (c): σ_θ; Panel (d): θ_0.

Figure 3 uses 20-point grids for the four jump-risk parameters and shows that the jump channel acts as a tail-risk channel with effects beyond drift compensation. Increasing λ raises the expected number of jump arrivals, so it affects the strike through two routes: more frequent variance jumps J^v lift future spot variance, and more frequent price jumps increase realized quadratic variation through $(e^{J^S} - 1)^2$. Increasing η raises the mean variance-jump size and therefore increases the expected integrated variance even if the price-jump distribution were unchanged. Increasing μ_J shifts the conditional price-jump distribution upward; because realized variance uses squared relative price jumps, both large positive and large negative jump multipliers are costly, but the exponential form makes positive jump means especially visible in the second moment. Finally, δ_J has the most clearly convex effect because it enters the second exponential moment as $e^{2\mu_J + 2\delta_J^2}$. Financially, this is the variance swap's well-known sensitivity to jump-tail thickness: the fair strike compensates the receiver of realized variance for rare but very large discontinuous price moves.

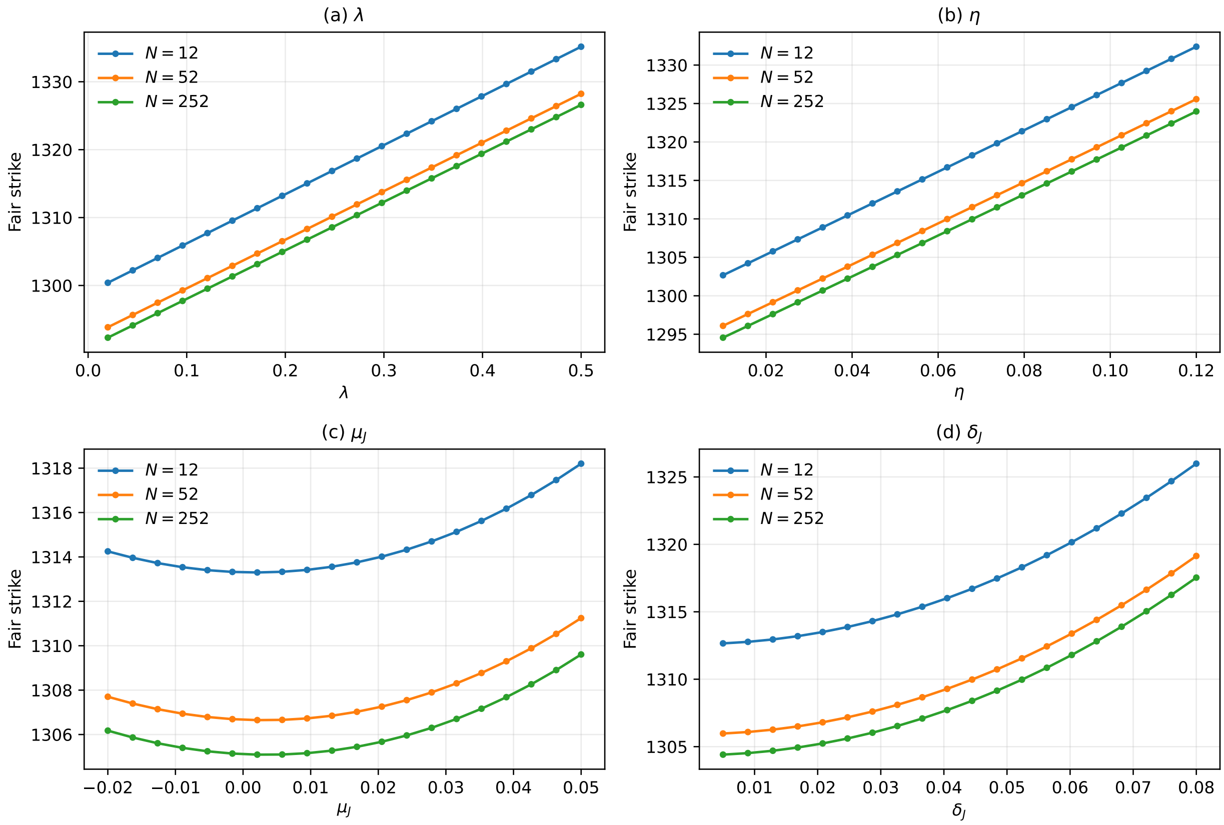

Figure 3. Sensitivity of the analytic fair strike to jump-risk parameters on 20-point parameter grids. Panel (a): λ; Panel (b): η; Panel (c): μ_J; Panel (d): δ_J.

7. Macro-liquidity contribution and robustness analysis

This section isolates the economic contribution of the macro-liquidity channel. Let the no-liquidity benchmark be obtained by setting $\alpha_y = 0$, with all other parameters unchanged. For the continuous-monitoring strike, define

$$A_v(T) = \frac{1 - e^{-\kappa_v T}}{\kappa_v}, \qquad A_y(T) = \frac{1 - e^{-\kappa_y T}}{\kappa_y}. \tag{7.1}$$

The contribution of the macro-liquidity channel to expected integrated variance is

$$I_y(T) = \alpha_y \bar{y}\big[T - A_v(T)\big] + \frac{\kappa_v \alpha_y (y_0 - \bar{y})}{\kappa_v - \kappa_y}\big[A_y(T) - A_v(T)\big], \tag{7.2}$$

and the corresponding continuous-monitoring fair-strike uplift is

$$\Delta K_y^c = \frac{100^2}{T} I_y(T). \tag{7.3}$$

Table 5 directly quantifies the marginal pricing contribution of the macro-liquidity channel by comparing the full model with the no-liquidity benchmark using the same analytic pricing routine as in the main numerical experiment. Across the two samples, the uplift is approximately 22–24 strike points, and the relative contribution is about 1.9% of the no-liquidity benchmark. This supports the interpretation that the new factor is economically visible and changes the expected variance path. The contribution is stable across the monitoring grid because it acts mainly through the expected path of future variance rather than through a purely sampling-frequency effect.

The first component, $\alpha_y \bar{y}[T - A_v(T)]$, measures the effect of the long-run macro-liquidity state on the long-run variance target. The second component measures how the initial liquidity disequilibrium $y_0 - \bar{y}$ affects the short- and medium-horizon path of the variance target. When liquidity stress raises the effective variance target, expected quadratic variation increases and the fair variance swap strike rises.

Table 5. Strike contribution of the macro-liquidity channel relative to the no-liquidity benchmark.

Sample	Frequency	Full model AS	No-liquidity AS	Difference	Difference (%)
Sample 1	Monthly ($N = 12$)	1163.4906	1141.0764	22.4141	1.9643
Sample 1	Fortnightly ($N = 26$)	1159.4636	1137.1822	22.2814	1.9594
Sample 1	Weekly ($N = 52$)	1157.7462	1135.5213	22.2248	1.9572
Sample 1	Daily ($N = 252$)	1156.3870	1134.2069	22.1801	1.9556
Sample 2	Monthly ($N = 12$)	1313.4335	1288.9977	24.4358	1.8957
Sample 2	Fortnightly ($N = 26$)	1308.7292	1284.4478	24.2814	1.8904
Sample 2	Weekly ($N = 52$)	1306.7397	1282.5236	24.2161	1.8882
Sample 2	Daily ($N = 252$)	1305.1731	1281.0086	24.1645	1.8864

Figure 4 plots the continuous-strike uplift implied by the decomposition. The neutral curve reflects the long-run component alone, while the easing and stress scenarios show how the initial deviation of liquidity conditions from equilibrium changes the short-horizon contribution. The stress curve lies above the neutral curve because $y_0 > \bar{y}$ raises the near-term effective variance target; the easing curve lies below it for the opposite reason.

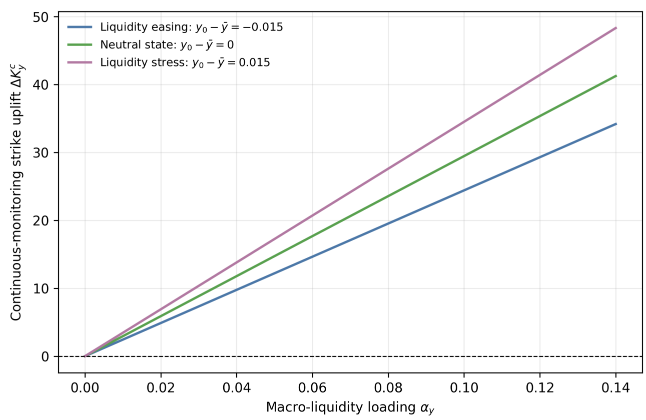

Figure 4. Continuous-monitoring strike uplift ΔK_y^c as a function of the macro-liquidity loading α_y under three liquidity-state scenarios: easing ($y_0 - \bar{y} = -0.015$), neutral ($y_0 - \bar{y} = 0$), and stress ($y_0 - \bar{y} = 0.015$). The figure uses the Sample 2 parameter set except for the displayed variation in α_y and $y_0 - \bar{y}$.

The Monte Carlo robustness experiment uses Sample 2 with weekly monitoring ($N = 52$), 100,000 simulated paths, and random seed 20260523. A substep is one Euler simulation step within a monitoring interval; for example, 10 substeps means that each weekly return interval is simulated on 10 finer time steps before the actual return is recorded at the monitoring date. Full truncation is used in all simulations to maintain numerical non-negativity of the variance process.

Table 6 provides a simulation-grid refinement diagnostic for the same actual-return realized variance definition as the analytic strike. The analytic weekly strike lies inside or very close to the reported 95% confidence intervals, and the relative errors remain small across grid refinements. The refinement therefore provides numerical support for the affine pricing implementation under the chosen admissible parameter regime, while analytical positivity remains governed by the finite-horizon restrictions stated above.

Table 6. Monte Carlo robustness under simulation-grid refinement for Sample 2 with weekly monitoring.

Substeps	MC estimate	Standard error	95% CI lower	95% CI upper	Analytic strike	Relative error (%)
1	1306.4024	0.8376	1304.7607	1308.0440	1306.7397	−0.0258
2	1305.0955	0.8332	1303.4625	1306.7286	1306.7397	−0.1258
5	1305.6331	0.8331	1304.0003	1307.2659	1306.7397	−0.0847
10	1306.5350	0.8303	1304.9077	1308.1624	1306.7397	−0.0157

8. Practical implications

The proposed macro-liquidity channel has several practical implications. First, it can be used by dealers and risk managers to adjust OTC variance swap quotes when market-wide liquidity or funding conditions deteriorate. Because the liquidity factor enters the variance target, its effect is persistent and extends beyond a one-period price discount. Second, the model provides a tractable device for volatility-risk management and stress testing of realized-variance exposure: different paths or initial levels of y_t translate into different expected quadratic-variation paths and hence different variance swap strikes. Third, observable financial-stress or market-liquidity indicators can be used as empirical proxies for y_t in future calibration work. Finally, the decomposition in Section 7 separates the long-run liquidity level effect from the initial liquidity-disequilibrium effect, which is useful for interpreting whether a variance-risk premium is driven by persistent market stress or by temporary liquidity shocks.

9. Conclusions

This paper studies variance swap valuation under a Heston-type stochastic-volatility jump model in which macro-liquidity conditions enter the variance mean-reversion target. The model preserves the affine structure despite the additional liquidity factor. We derive the joint moment-generating function, the associated Riccati system, the fair strike of discretely sampled actual-return variance swaps, and the continuously monitored limiting strike. We also state finite-horizon transform admissibility conditions and prove that the discrete actual-return strike converges to the continuous quadratic-variation benchmark as the monitoring mesh tends to zero.

The main economic conclusion is that macro-liquidity affects variance swap pricing through expected future quadratic variation. When liquidity stress raises the effective target $\theta_t + \alpha_y y_t$, the expected path of v_t increases and the fair variance swap strike rises. The continuous-strike decomposition shows that the long-run liquidity component contributes through $\alpha_y \bar{y}[T - A_v(T)]$, while the initial liquidity disequilibrium contributes through the transient variance-target path.

The numerical results support the analytical formulas and clarify the size of the new channel. The model reduces to the no-liquidity and no-jump reference specifications under the corresponding parameter restrictions. In the benchmark calibration, the macro-liquidity channel raises the fair strikes by approximately 22–24 strike points, corresponding to about 1.9% of the no-liquidity benchmark. Monte Carlo estimates remain close to the affine-transform prices, and the discrete strikes move toward the continuous-monitoring benchmark as the sampling frequency increases. The robustness experiment further indicates that the full-truncation simulation scheme is numerically stable under grid refinement.

The model has limitations that also suggest future research directions. Since θ_t and y_t are Gaussian Ornstein–Uhlenbeck factors, the effective variance target is not globally constrained to be positive. The pricing formulas should therefore be interpreted on the finite-horizon moment domain established in this paper. Future work may replace the Gaussian liquidity factor with a positive factor, calibrate the model to observable market-liquidity proxies and option-implied variance data, and study hedging performance under liquidity stress.

Author contributions

All authors contributed equally to the conception and design of the study, data analysis, manuscript writing, and final approval of the published version.

Use of Generative-AI tools declaration

The authors declare that they have not used Artificial Intelligence (AI) tools in the creation of this article.

Acknowledgements

This work was supported by the Fundamental Research Funds for the Central Universities, Grant Number 25CAFUC04077, under the research project "The Effect of Long Memory in Hawkes Jump Risks on Generalized Variance Swap Pricing within a Stochastic Liquidity Risk Framework", and the Natural Science Foundation of Sichuan Province (Grant No. 2025ZNSFSC0818).

Conflict of interest

We declare that we have no conflict of interest.

References

1. E. O. Abensur, R. Saigal, S. Zhang, Y. Song, H. Yu, Stochastic liquidity model and its applications to portfolio selection, In: *Proceedings on 25th International Joint Conference on Industrial Engineering and Operations Management–IJCIEOM*, Springer, 2020, 42–51. http://doi.org/10.1007/978-3-030-43616-2_5

2. O. E. Barndorff-Nielsen, N. Shephard, Power and bipower variation with stochastic volatility and jumps, *J. Financ. Economet.*, **2** (2004), 1–37. http://doi.org/10.1093/jjfinec/nbh001

3. D. S. Bates, Jumps and stochastic volatility: Exchange rate processes implicit in Deutsche Mark options, *Rev. Financ. Stud.*, **9** (1996), 69–107. http://doi.org/10.1093/rfs/9.1.69

4. J. F. Bégin, C. Dorion, G. Gauthier, Idiosyncratic jump risk matters: Evidence from equity returns and options, *Rev. Financ. Stud.*, **33** (2020), 155–211. http://doi.org/10.1093/rfs/hhz043

5. M. Brenner, R. Eldor, S. Hauser, The price of options illiquidity, *J. Financ.*, **56** (2001), 789–805. http://doi.org/10.1111/0022-1082.00346

6. M. Broadie, A. Jain, The effect of jumps and discrete sampling on volatility and variance swaps, *Int. J. Theor. Appl. Fin.*, **11** (2008), 761–797. http://doi.org/10.1142/S0219024908005032

7. W. Chen, F. Zhou, X. J. He, Analytically pricing commodity futures options under financialization with stochastic liquidity risks, *J. Futures Markets*, **46** (2026), 1154–1166. http://doi.org/10.1002/fut.70103

8. Z. Cui, J. L. Kirkby, D. Nguyen, A general framework for discretely sampled realized variance derivatives in stochastic volatility models with jumps, *Eur. J. Oper. Res.*, **262** (2017), 381–400. http://doi.org/10.1016/j.ejor.2017.04.007

9. D. Duffie, J. Pan, K. Singleton, Transform analysis and asset pricing for affine jump-diffusions, *Econometrica*, **68** (2000), 1343–1376. http://doi.org/10.1111/1468-0262.00164

10. R. J. Elliott, T. K. Siu, L. Chan, J. W. Lau, Pricing options under a generalized Markov-modulated jump-diffusion model, *Stoch. Anal. Appl.*, **25** (2007), 821–843. http://doi.org/10.1080/07362990701420118

11. C. Ewald, Y. Zou, Analytic formulas for futures and options for a linear quadratic jump diffusion model with seasonal stochastic volatility and convenience yield: Do fish jump? *Eur. J. Oper. Res.*, **294** (2021), 801–815. http://doi.org/10.1016/j.ejor.2021.02.004

12. S. P. Feng, M. W. Hung, Y. H. Wang, Option pricing with stochastic liquidity risk: Theory and evidence, *J. Financ. Mark.*, **18** (2014), 77–95. http://doi.org/10.1016/j.finmar.2013.05.002

13. J. Fu, Analytic solutions of variance swaps for Heston models with stochastic long-run mean of variance and jumps, *PLOS ONE*, **20** (2025), e0318886. http://doi.org/10.1371/journal.pone.0318886

14. X. J. He, W. Chen, A closed-form pricing formula for European options under a new stochastic volatility model with a stochastic long-term mean, *Math. Finan. Econ.*, **15** (2021), 381–396. http://doi.org/10.1007/s11579-020-00281-y

15. X. J. He, S. Lin, Volatility swaps valuation under a modified risk-neutralized Heston model with a stochastic long-run variance level, *ANZIAM J.*, **64** (2022), 250–263. http://doi.org/10.1017/S144618112200013X

16. X. J. He, S. Lin, Analytical formulae for variance and volatility swaps with stochastic volatility, stochastic equilibrium level and regime switching, *AIMS Mathematics*, **9** (2024), 22225–22238. http://doi.org/10.3934/math.20241081

17. X. J. He, S. Lin, A stochastic liquidity risk model with stochastic volatility and its applications to option pricing, *Stoch. Models*, **41** (2025), 273–292. http://doi.org/10.1080/15326349.2024.2332326

18. S. L. Heston, A closed-form solution for options with stochastic volatility with applications to bond and currency options, *Rev. Financ. Stud.*, **6** (1993), 327–343. http://doi.org/10.1093/rfs/6.2.327

19. Z. Hu, B. Z. Yang, X. J. He, J. Yue, Equilibrium pricing of European crude oil options with stochastic behaviour and jump risks, *Math. Comput. Simulat.*, **219** (2024), 212–230. http://doi.org/10.1016/j.matcom.2023.12.020

20. M. A. Keene, D. R. Peterson, The importance of liquidity as a factor in asset pricing, *J. Financ. Res.*, **30** (2007), 91–109. http://doi.org/10.1111/j.1475-6803.2007.00204.x

21. H. Mesgarani, Y. E. Aghdam, A. Beiranvand, J. F. Gómez-Aguilar, A novel approach to fuzzy based efficiency assessment of a financial system, *Comput. Econ.*, **63** (2024), 1609–1626. http://doi.org/10.1007/s10614-023-10376-5

22. P. Pasricha, X. J. He, Exchange options with stochastic liquidity risk, *Expert Syst. Appl.*, **223** (2023), 119915. http://doi.org/10.1016/j.eswa.2023.119915

23. L. Pástor, R. F. Stambaugh, Liquidity risk and expected stock returns, *J. Polit. Econ.*, **111** (2003), 642–685. http://doi.org/10.1086/374184

24. X. Wang, S. Song, Y. Wang, The valuation of power exchange options with counterparty risk and jump risk, *J. Futures Markets*, **37** (2017), 499–521. http://doi.org/10.1002/fut.21803

25. K. Wang, X. X. Guo, H. Y. Zhang, Valuations of generalized variance swaps under the jump-diffusion model with stochastic liquidity risk, *N. Am. J. Econ. Finance*, **73** (2024), 102190. http://doi.org/10.1016/j.najef.2024.102190

26. J. Wu, J. F. Gómez-Aguilar, R. Taleghani, Portfolio optimization under the uncertain financial model, *Comput. Econ.*, **66** (2025), 571–592. http://doi.org/10.1007/s10614-024-10727-w

27. D. Xu, B. Yang, J. Kang, N. Huang, Variance and volatility swaps valuations with the stochastic liquidity risk, *Physica A*, **566** (2021), 125679. http://doi.org/10.1016/j.physa.2020.125679

28. Y. Yoon, J. H. Seo, J. H. Kim, Closed-form pricing formulas for variance swaps in the Heston model with stochastic long-run mean of variance, *Comput. Appl. Math.*, **41** (2022), 235. http://doi.org/10.1007/s40314-022-01939-7

29. T. S. Zaevski, Y. S. Kim, F. J. Fabozzi, Option pricing under stochastic volatility and tempered stable Lévy jumps, *Int. Rev. Financ. Anal.*, **31** (2014), 101–108. http://doi.org/10.1016/j.irfa.2013.10.004

30. H. Zhang, X. Guo, K. Wang, S. Huang, The valuation of American options with the stochastic liquidity risk and jump risk, *Physica A,* **650** (2024), 129911. http://doi.org/10.1016/j.physa.2024.129911

31. S. P. Zhu, G. H. Lian, On the valuation of variance swaps with stochastic volatility, *Appl. Math. Comput.*, **219** (2012), 1654–1669. http://doi.org/10.1016/j.amc.2012.08.006

A. Supplementary

A.1. Proof of Lemma 1

Proof. At maturity $\tau = 0$, the terminal condition is

$$U(0, x, v, \vartheta, y; \phi, b, c, f, \gamma) = \exp(\phi x + bv + c\vartheta + fy + \gamma). \tag{A.1}$$

Applying Ito's formula to $x_t = \ln S_t$ gives the log-price dynamics

$$dx_t = \left(r - d - \lambda m - \frac{1}{2}v_t\right) dt + \sqrt{v_t}\, dW_t^S + J^S\, dN_t. \tag{A.2}$$

The Feynman–Kac PIDE for $U(\tau, x, v, \vartheta, y; \phi, b, c, f, \gamma)$ is therefore

$$\begin{aligned}\frac{\partial U}{\partial \tau} &= \left(r - d - \lambda m - \frac{v}{2}\right)\frac{\partial U}{\partial x} + \kappa_v(\vartheta + \alpha_y y - v)\frac{\partial U}{\partial v} + \kappa_\theta(\bar{\theta} - \vartheta)\frac{\partial U}{\partial \vartheta} + \kappa_y(\bar{y} - y)\frac{\partial U}{\partial y}\\ &\quad + \frac{v}{2}\frac{\partial^2 U}{\partial x^2} + \frac{\sigma_v^2 v}{2}\frac{\partial^2 U}{\partial v^2} + \frac{\sigma_\theta^2}{2}\frac{\partial^2 U}{\partial \vartheta^2} + \frac{\sigma_y^2}{2}\frac{\partial^2 U}{\partial y^2} + \rho_{sv}\sigma_v v\frac{\partial^2 U}{\partial x \partial v}\\ &\quad + \lambda\mathbb{E}^{\mathbb{Q}}\left[U(\tau, x + J^S, v + J^v, \vartheta, y; \phi, b, c, f, \gamma) - U(\tau, x, v, \vartheta, y; \phi, b, c, f, \gamma)\right].\end{aligned} \tag{A.3}$$

Substituting the affine ansatz (3.2) into (A.3) and collecting the coefficients of v, ϑ, y, and the constant term gives

$$\begin{cases} B'(\tau) = -\frac{1}{2}(\phi - \phi^2) - (\kappa_v - \rho_{sv}\sigma_v\phi)B(\tau) + \frac{1}{2}\sigma_v^2 B^2(\tau),\\ C'(\tau) = \kappa_v B(\tau) - \kappa_\theta C(\tau),\\ F'(\tau) = \alpha_y\kappa_v B(\tau) - \kappa_y F(\tau),\\ D'(\tau) = (r - d)\phi + \kappa_\theta\bar{\theta}C(\tau) + \kappa_y\bar{y}F(\tau) + \frac{1}{2}\sigma_\theta^2 C^2(\tau) + \frac{1}{2}\sigma_y^2 F^2(\tau),\\ E'(\tau) = \lambda\left(\dfrac{\exp\left(\phi\mu_J + \frac{1}{2}\phi^2\delta_J^2\right)}{1 - \eta\left(B(\tau) + \phi\rho_J\right)} - 1 - m\phi\right). \end{cases} \tag{A.4}$$

with initial conditions

$$B(0) = b, \qquad C(0) = c, \qquad F(0) = f, \qquad D(0) = \gamma, \qquad E(0) = 0. \tag{A.5}$$

Solving the scalar Riccati equation for B and then the linear equations for C and F, with D and E obtained by integration, yields (3.4)–(3.8). □

A.2. Proof of Proposition 1

Proof. We give the details because the admissibility restrictions determine the moment domain of the discrete-strike formula. For fixed ϕ, the coefficient B satisfies a scalar Riccati equation whose coefficients are continuous and locally Lipschitz in B. Hence, the solution is unique up to the first possible explosion time. In the explicit representation used in Lemma 1, such an explosion can occur only when the Riccati denominator vanishes. Once the B-trajectory is finite on a given finite interval, the remaining possible source of transform failure is the jump-exponential term in E, whose finiteness is governed by the jump-transform denominator.

The jump transform can be computed explicitly. Conditional on J^v, the price jump J^S is normally distributed with mean $\mu_J + \rho_J J^v$ and variance δ_J^2. Therefore, for any real ϕ and B,

$$\mathbb{E}\left[\exp\{\phi J^S + BJ^v\}\right] = \exp\left(\phi\mu_J + \frac{1}{2}\phi^2\delta_J^2\right)\mathbb{E}[\exp\{(B + \phi\rho_J)J^v\}] = \frac{\exp\left(\phi\mu_J + \frac{1}{2}\phi^2\delta_J^2\right)}{1 - \eta(B + \phi\rho_J)}. \tag{A.6}$$

Thus, the transform is finite exactly on the half-space

$$1 - \eta(B + \phi\rho_J) > 0. \tag{A.7}$$

For the first-stage transforms used in the discrete variance-swap formula, $\phi = p \in \{1, 2\}$ and $B = B_p(s)$, which gives the conditions $1-\eta(B_p(s)+p\rho_J) > 0$ for $0 \le s \le T$. The separate inequalities $1-\rho_J\eta > 0$ and $1 - 2\rho_J\eta > 0$ ensure the finiteness of the first and second exponential jump moments entering the compensator and the jump quadratic-variation term.

For the second tower-property transform, $\phi = 0$ and $B = \widehat{B}_p(s; \Delta)$, which gives the condition $1 - \eta\widehat{B}_p(s; \Delta) > 0$ for $0 \le s \le T$. Under these restrictions and the non-vanishing of the explicit Riccati denominator, B_p and $\widehat{B}_p$ remain finite on the finite interval under consideration. The coefficients C and F solve linear inhomogeneous equations driven by B, while D and E are finite integrals of continuous functions of the admissible Riccati trajectory. Therefore, all affine coefficients used in Lemma 1 and in the two transforms of Theorem 1 are finite.

It follows that $M_1(t; \Delta)$ and $M_2(t; \Delta)$ are finite for every monitoring date and that the summands in the discrete actual-return variance swap strike are well defined. This proves that the two exponential transforms required for $M_1(t; \Delta)$ and $M_2(t; \Delta)$ are finite on the monitoring grid, which is precisely the admissibility condition needed for the discrete actual-return variance swap strike. □

A.3. Proof of Theorem 1

Proof. From $S_t = e^{x_t}$ we have $\frac{S_{t_i}-S_{t_{i-1}}}{S_{t_{i-1}}} = e^{x_{t_i}-x_{t_{i-1}}} - 1$, so squaring yields (4.3). For a fixed $p \in \{1, 2\}$, let U_p denote the transform defined in Lemma 1 with initial vector $(\phi, b, c, f, \gamma) = (p, 0, 0, 0, 0)$. By the tower property,

$$\begin{aligned}\mathbb{E}^{\mathbb{Q}}\left[e^{p(x_{t_i}-x_{t_{i-1}})} \mid \mathcal{F}_{t_{i-1}}\right] &= e^{-px_{t_{i-1}}}\,\mathbb{E}^{\mathbb{Q}}\left[e^{px_{t_i}} \mid \mathcal{F}_{t_{i-1}}\right] \\ &= e^{-px_{t_{i-1}}}\,U_p\big(\Delta, x_{t_{i-1}}, v_{t_{i-1}}, \theta_{t_{i-1}}, y_{t_{i-1}}; p, 0, 0, 0, 0\big).\end{aligned} \tag{A.8}$$

Substituting the affine representation of U_p over the interval $[t_{i-1}, t_i]$ cancels the factor $e^{px_{t_{i-1}}}$ and gives

$$\mathbb{E}^{\mathbb{Q}}\left[e^{p(x_{t_i}-x_{t_{i-1}})} \mid \mathcal{F}_{t_{i-1}}\right] = \exp\Big(B_p^\Delta v_{t_{i-1}} + C_p^\Delta\theta_{t_{i-1}} + F_p^\Delta y_{t_{i-1}} + D_p^\Delta + E_p^\Delta\Big). \tag{A.9}$$

Taking the unconditional expectation and applying Lemma 1 again with $\phi = 0$ and initial coefficients $(b, c, f) = (B_p^\Delta, C_p^\Delta, F_p^\Delta)$ yields

$$\mathbb{E}^{\mathbb{Q}}\left[\exp\Big(B_p^\Delta v_{t_{i-1}} + C_p^\Delta\theta_{t_{i-1}} + F_p^\Delta y_{t_{i-1}} + D_p^\Delta + E_p^\Delta\Big)\right]$$

$$= \exp\Big(D_p^{\Delta} + E_p^{\Delta} + \widehat{B}_p(t_{i-1};\Delta)v_0 + \widehat{C}_p(t_{i-1};\Delta)\theta_0 + \widehat{F}_p(t_{i-1};\Delta)y_0 + \widehat{D}_p(t_{i-1};\Delta) + \widehat{E}_p(t_{i-1};\Delta)\Big) = \mathcal{M}_p(t_{i-1};\Delta). \tag{A.10}$$

Inserting the cases $p = 2$ and $p = 1$ into the expansion of the squared return and summing over $i = 1,\dots,N$ gives (4.6). The cancellation of all $x_{t_{i-1}}$ terms confirms the scale invariance of actual-return sampling, consistent with the definition of the realized return. As a consistency check, for $p = 1$ and $(b, c, f) = (0, 0, 0)$ the Riccati system yields $B_1^{\Delta} = C_1^{\Delta} = F_1^{\Delta} = E_1^{\Delta} = 0$ and $D_1^{\Delta} = (r - d)\Delta$; hence $\mathcal{M}_1(t;\Delta) = e^{(r-d)\Delta}$, which matches the risk-neutral conditional mean $\mathbb{E}^{\mathbb{Q}}[S_{t+\Delta}/S_t \mid \mathcal{F}_t]$. □

A.4. Proof of Theorem 2

Proof. The proof proceeds by computing the expectation of each component of RV_T^c. The Ornstein–Uhlenbeck processes for θ_t and y_t satisfy

$$\frac{d}{dt}\mathbb{E}[\theta_t] = \kappa_\theta(\bar{\theta} - \mathbb{E}[\theta_t]), \qquad \frac{d}{dt}\mathbb{E}[y_t] = \kappa_y(\bar{y} - \mathbb{E}[y_t]),$$

so that

$$\mathbb{E}[\theta_t] = \bar{\theta} + (\theta_0 - \bar{\theta})e^{-\kappa_\theta t}, \qquad \mathbb{E}[y_t] = \bar{y} + (y_0 - \bar{y})e^{-\kappa_y t}. \tag{A.11}$$

The variance process v_t includes jumps with mean $\mathbb{E}[J^v] = \eta$; its dynamics imply

$$\frac{d}{dt}\mathbb{E}[v_t] = \kappa_v\big(\mathbb{E}[\theta_t] + \alpha_y\mathbb{E}[y_t] - \mathbb{E}[v_t]\big) + \lambda\eta.$$

Substituting the expectations of θ_t and y_t yields

$$\frac{d}{dt}\mathbb{E}[v_t] + \kappa_v\mathbb{E}[v_t] = \kappa_v(\bar{\theta} + \alpha_y\bar{y}) + \lambda\eta + \kappa_v(\theta_0 - \bar{\theta})e^{-\kappa_\theta t} + \kappa_v\alpha_y(y_0 - \bar{y})e^{-\kappa_y t}.$$

Multiplying by the integrating factor $e^{\kappa_v t}$ and integrating from 0 to t gives

$$\mathbb{E}[v_t] = \bar{v}_\infty(1 - e^{-\kappa_v t}) + v_0 e^{-\kappa_v t} + \frac{\kappa_v(\theta_0 - \bar{\theta})}{\kappa_v - \kappa_\theta}\big(e^{-\kappa_\theta t} - e^{-\kappa_v t}\big) + \frac{\kappa_v\alpha_y(y_0 - \bar{y})}{\kappa_v - \kappa_y}\big(e^{-\kappa_y t} - e^{-\kappa_v t}\big). \tag{A.12}$$

Integrating $\mathbb{E}[v_t]$ over $[0, T]$ yields the first four terms of the expression for K_{var}^c (the terms without J_2).

For the jump contribution, the conditional moment generating function of J^S given J^v is

$$\mathbb{E}[e^{pJ^S}] = \frac{\exp(p\mu_J + p^2\delta_J^2/2)}{1 - p\rho_J\eta}, \qquad p = 1, 2. \tag{A.13}$$

Hence,

$$\mathbb{E}\big[(e^{J^S} - 1)^2\big] = \mathbb{E}[e^{2J^S}] - 2\mathbb{E}[e^{J^S}] + 1 = J_2. \tag{A.14}$$

Because the jump sizes are i.i.d. and independent of the Poisson counting process N_T,

$$\mathbb{E}^{\mathbb{Q}}\left[\sum_{i=1}^{N_T}(e^{J_i^S}-1)^2\right]=\lambda T J_2. \tag{A.15}$$

Assembling all parts gives the stated formula for K_{var}^c. Setting $t=0$ in $\mathbb{E}[v_t]$ recovers v_0, and differentiating the expression reproduces the linear mean equation. Moreover, the jump moments coincide with the transform in Lemma 1 for $\phi=1,2$ and $B=0$, confirming that the same transform domain is used throughout. □

A.5. Proof of Theorem 3

Proof. Define the relative price return semimartingale Y_t by $Y_t=\int_0^t \frac{dS_s}{S_{s-}}$. Under the asset price dynamics,

$$Y_t=\int_0^t(r-d-\lambda m)\,ds+\int_0^t\sqrt{v_s}\,dW_s^S+\sum_{0<s\le t}(e^{J_s^S}-1), \tag{A.16}$$

where $m=\mathbb{E}[e^{J^S}-1]$. Its continuous local martingale part is $\int_0^t\sqrt{v_s}\,dW_s^S$, so the continuous quadratic variation is $[Y]_t^c=\int_0^t v_s\,ds$. At a jump time s, the jump size of Y is $\Delta Y_s=\Delta S_s/S_{s-}=e^{J_s^S}-1$. Hence, the full quadratic variation equals

$$[Y]_T=[Y]_T^c+\sum_{0<s\le T}(\Delta Y_s)^2=\int_0^T v_s\,ds+\sum_{i=1}^{N_T}(e^{J_i^S}-1)^2. \tag{A.17}$$

For any cadlag semimartingale, the realized quadratic variation along a deterministic partition with mesh tending to zero converges in probability to the quadratic variation

$$\sum_{i=1}^{N}(Y_{t_i}-Y_{t_{i-1}})^2\xrightarrow{\mathbb{P}}[Y]_T. \tag{A.18}$$

However, the discrete variance swap uses the simple return $R_i^{(S)}=(S_{t_i}-S_{t_{i-1}})/S_{t_{i-1}}$, whereas $Y_{t_i}-Y_{t_{i-1}}=\int_{t_{i-1}}^{t_i}dS_s/S_{s-}$. We compare the two quantities on each interval.

On an interval containing no jump, Ito's expansion gives

$$R_i^{(S)}-(Y_{t_i}-Y_{t_{i-1}})=O_{\mathbb{P}}(t_i-t_{i-1}), \tag{A.19}$$

because both terms share the same first-order stochastic increment $\sqrt{v_{t_{i-1}}}(W_{t_i}^S-W_{t_{i-1}}^S)$. Summing the squared differences over all jump-free intervals yields an error of order $O_{\mathbb{P}}(|\Pi_N|)$, using the finite second moments of v_t.

On an interval containing a jump, the Poisson process has only finitely many jumps on $[0,T]$ almost surely. As $|\Pi_N|\to 0$, each jump s becomes isolated in a unique interval whose length shrinks to zero, so that

$$R_i^{(S)}\to e^{J_s^S}-1 \tag{A.20}$$

for that interval. The probability of two or more jumps in a single interval is $O((t_i-t_{i-1})^2)$, and $\sum_i O((t_i-t_{i-1})^2)\le T|\Pi_N|\,O(1)$; hence, such intervals contribute negligibly in the limit.

Combining the continuous and jump arguments, we obtain

$$\sum_{i=1}^{N}\left(\frac{S_{t_i}-S_{t_{i-1}}}{S_{t_{i-1}}}\right)^2 \xrightarrow{\mathbb{P}} \int_0^T v_s\,ds+\sum_{i=1}^{N_T}(e^{J_i^S}-1)^2. \tag{A.21}$$

The moment conditions (finite exponential moments up to order two and integrability of v_t) imply uniform integrability of the realised variance sequence. Therefore, convergence in probability upgrades to L^1 convergence

$$\lim_{|\Pi_N|\to 0}\mathbb{E}^{\mathbb{Q}}\left[\sum_{i=1}^{N}\left(\frac{S_{t_i}-S_{t_{i-1}}}{S_{t_{i-1}}}\right)^2\right]=\mathbb{E}^{\mathbb{Q}}\left[\int_0^T v_s\,ds+\sum_{i=1}^{N_T}(e^{J_i^S}-1)^2\right]. \tag{A.22}$$

Multiplying by $100^2/T$ gives the claimed limit $K_{\mathrm{var}}^{(1)}(\Pi_N)\to K_{\mathrm{var}}^{c}$ as $|\Pi_N|\to 0$. □